Nonlinear Seasonal and Long-Term Trends in a Twentieth-Century Meteorological Drought Index across the Continental United States

KYUNGMIN SUNG[a] AND JAMES H. STAGGE[a]

[a] *Department of Civil, Environmental and Geodetic Engineering, The Ohio State University, Columbus, Ohio*

(Manuscript received 18 January 2022, in final form 18 May 2022)

ABSTRACT: Analyzing gradual trends in meteorological drought has become increasingly important as anthropogenic climate change and natural climate variability interact to complicate measurement of drought severity. Complex seasonality and long-term trends pose a limitation in understanding spatial trends in nonstationary changes of meteorological drought in the United States. This study seeks to address this issue by simultaneously analyzing recurring seasonal patterns (stationary component) and long-term drought trends (nonstationary component), with a unique focus on nonlinear trends and common regional patterns. We analyzed 696 instrumental precipitation gauges with long historical records in the continental United States, using a novel spline-based model to disaggregate a 3-month meteorological drought index (SPI) into its seasonal and long-term components. The disaggregated components for each gauge were then clustered into subregions with similar seasonality and groupings with similar long-term trends using a two-step process. Our results identify clearly defined regions based on precipitation seasonality, while long-term trends are not spatially coherent with the seasonality. Instead, these findings support prior findings of an increasingly drier western United States and an increasingly wetter eastern United States over the last century, but with more nuanced spatial and temporal patterns. The new clustering analysis based on nonstationary meteorological drought trends can contribute to informing and adapting current water management strategies to long-term drought trends.

SIGNIFICANCE STATEMENT: This study considered 656 precipitation gauges across the continental United States to find regions with similar precipitation seasonality and then to group records with similar long-term climate trends. The study focused on 3-month average precipitation, a key indicator for drought monitoring. We identified eight regions across the United States with similar precipitation seasonality. From 1920 to the present, we found continuous drying trends throughout the western United States, continuously wetter trends in the northern plains, and an overall wetter trend interrupted by a midcentury dry period (1930–50) for much of the central Plains and Midwest. This study's use of splines, or fitted curves, allowed these nonlinear patterns, which we believe better capture the nuances and intensification of climate change effects on precipitation.

KEYWORDS: Drought; Seasonal cycle; Trends; Precipitation; Multidecadal variability; Clustering

1. Introduction

Drought trends have long been studied as a primary issue in water management, especially as related to modern anthropogenic climate change (Trenberth et al. 2014; Ukkola et al. 2020; Cook et al. 2019). Climate change has induced complicated shifts in the severity and frequency of drought (Cook et al. 2019; Dai et al. 2018; Seager et al. 2009; Cook et al. 2010) and those changes vary across regions and seasons (Cook et al. 2010; Diffenbaugh 2020; Stahle 2020; Seneviratne 2012; Sheffield et al. 2012; Cook et al. 2020). For example, the southwestern United States and the Mediterranean region of Europe have experienced increasingly drier patterns during the last century, while northern Europe and the Midwestern United States have become wetter (Hoerling et al. 2012; Stagge et al. 2017). The commonly repeated adage of "dry gets drier and wet gets wetter" provides a simple shorthand, but it is too simplified to explain more nuanced regional trends or seasonal-specific drought trends, or does not hold in some land areas (Hu et al. 2019; Chou et al. 2013; Byrne and O'Gorman 2015). These drought trends impact water security and the ecosystem, posing challenges to water resource management, while also providing insight into anthropogenic climate change impacts, and therefore are important to investigate in greater detail.

The definition of drought can vary depending on what part of the hydrologic cycle is of interest. For example, meteorological drought measures anomalies in precipitation, hydrological drought measures streamflow anomalies, and agricultural drought measures soil moisture or agriculture yield anomalies (Lloyd-Hughes and Saunders 2002). Because each drought type focuses on a specific part of the hydrologic cycle, they can have unique impacts in addition to onset/cessation characteristics (Heim 2002; Mishra and Singh 2010). This study focuses on meteorological drought, defined as a lack of precipitation relative to typical conditions prolonged for a certain time period (Lloyd-Hughes and Saunders 2002; Stagge et al. 2015a; McKee et al. 1993). Measuring only precipitation, meteorological drought is often the primary cause of other types of drought as this anomaly propagates through the hydrologic cycle to induce water balance (precipitation minus evapotranspiration) (Palmer 1965; Stagge et al. 2015b), hydrologic (Van Loon et al. 2015), agricultural, and socioeconomic droughts (Ukkola et al. 2020; McKee et al. 1993;

Corresponding author: James H. Stagge, stagge.11@osu.edu

DOI: 10.1175/JCLI-D-22-0045.1

Van Loon et al. 2016). The Standardized Precipitation Index (SPI) is commonly used to quantify the severity of meteorological drought using only precipitation, while indices like the Standard Precipitation Evaporation Index (SPEI) or Palmer Drought Severity Index (PDSI) measure water balance and agricultural drought by considering evapotranspiration or simplified soil behavior (Mishra and Singh 2010; Vicente-Serrano et al. 2010; McKee et al. 1993; Lloyd-Hughes and Saunders 2002).

The SPI measures drought severity using only precipitation and is calculated by fitting precipitation records of an accumulated duration (e.g., 1, 3, 6, or 12 months) to a probability density function, generally the gamma distribution or Pearson type III distribution (Mishra and Singh 2010; McKee et al. 1993; Stagge et al. 2015b). Then, the calculated probability is standardized by being transformed to the standard normal distribution (Heim 2002; Guttman 1999). Since the SPI is normalized based on the historical record, we can interpret the values as the normalized anomaly from the region's observed long-term mean. In other words, the SPI enables the user to compare drought severity relative to a location's long-term climatology across different locations and time scales (Lloyd-Hughes and Saunders 2002; Guttman 1999). This index therefore mirrors the definition of meteorological drought as an extended anomaly from typical conditions. In addition, 3-month SPI reflects seasonal characteristics in temperate climate zones with four distinct seasons (Vicente-Serrano et al. 2021). Even those regions with fewer distinct seasons or seasons lasting longer than 3 months should be adequately captured by a 3-month moving average with a daily time step. There have been critiques that SPI measures drought using only precipitation without incorporating water loss or evapotranspiration (Vicente-Serrano et al. 2010). Nevertheless, the SPI has proven to perform well relative to its simple data requirement (i.e., precipitation only and a straightforward calculation process) (Ukkola et al. 2020; Lloyd-Hughes and Saunders 2002; McKee et al. 1993; Heim 2002). Isolating a single variable like precipitation to calculate a drought index provides a more straightforward interpretation, linking the variable (precipitation) and the measurement (drought severity). Also, the simplicity leads to more easily understood uncertainty estimates compared to indices that also incorporate evapotranspiration or soil moisture, which in turn are composed of temperature, wind speed, or soil characteristics, each with their own biases and measurement error (Ukkola et al. 2020). There cannot be a best single index to perfectly measure drought as there is no single fixed definition to describe droughts for all circumstances (Lloyd-Hughes 2014). In light of these considerations, the SPI with a gamma distribution and 3-month accumulation period was chosen for this study and used to explain both seasonal and long-term characteristics of meteorological drought.

This study analyzes spatiotemporal trends in the meteorological drought index SPI over the continental United States during the twentieth-century instrumental period. Because this index was originally designed as a drought index, we will continue to refer to meteorological drought; however, this index measures both drought (negative SPI) and pluvials (positive SPI). Therefore, a change in the mean parameter of the SPI-3 technically indicates a shift toward wetter or dryer conditions for seasonal (3-month) precipitation. Prior studies show a general consensus in precipitation and drought trends across the continental United States during this period, with increasing dryness in the western United States and increasing wetness in the eastern United States (Andreadis and Lettenmaier 2006; Herweijer et al. 2007; Cook et al. 2015). Major record-breaking drought events during the instrumental period include the Dust Bowl (1930s) and the southern Great Plains drought (1950s), while extreme drought trends in the southwest region have made the reoccurrence of similar extreme events more likely and frequent in recent decades (Cook et al. 2010; Stahle 2020; Williams et al. 2020). Future projections of climate change suggest current trends will continue throughout the next century (Ukkola et al. 2020; Cook et al. 2020). Cook et al. (2020) predicted future drought trends in the United States by comparing projected PDSI during 2071–2100 to 1851–80 using CMIP6 forcing scenarios. They show that changes in drought trend will likely vary by season and region, with the cold season in the eastern part of the United States tending toward wetter conditions and the warm season in the U.S. Southwest tending to have a drier trend. Ukkola et al. (2020) predicted complicated patterns of future change in drought using CMIP6 projections by comparing the average drought of 2051–2100 to the base period 1950–2014 across the United States. They found that future change will mostly occur in seasonality shifts and the frequency of extreme drought events while changes in drought intensity will not be significant. Marvel et al. (2021) also found regions in the United States with projected future changes in seasonal and long-term precipitation. For example, the Southeast is likely to undergo an increase in the amplitude of the annual precipitation cycle, making both high and low values more extreme, while the upper Great Plains tends to undergo shifts in the annual peak precipitation season. While model-derived projections of precipitation are more uncertain than variables like temperature (Vicente-Serrano et al. 2021; Lee et al. 2019), studies have shown consistent regional results (Ukkola et al. 2020) and the sign agreement between historical observations and future projections provides some additional confidence. These projected future changes in the literature highlight the importance of understanding regional drought trends in both seasonal and long-term time scales.

Statistical approaches for quantifying long-term drought trends typically rely on one of two approaches: either to calculate the rate of gradual, monotonic change over time or to calculate the step difference between two nonoverlapping time periods (Helsel et al. 2020). For analyzing monotonic change, linear regression or the Mann–Kendall (MK) trend tests are the most widely used methods (Rahmani et al. 2015; Ganguli and Ganguly 2016). Linear regression is the simplest method, performed by calculating the slope of a regression line relative to time and testing its statistical significance by comparing the estimated slope to a slope of zero (the null hypothesis). Since simple linear regression assumes the data are normally distributed about the regression line and have uniform variance, it has a limitation to model highly skewed data such as

precipitation directly. The MK test can be used as an alternative. It is particularly robust for hydroclimate data as it is a nonparametric test, which is free from the normality assumption and is less sensitive to high leverage outliers (Mann 1945; Andreadis and Lettenmaier 2006). For calculating a step difference between two periods, the *t* test and Mann–Whitney test are popular parametric and nonparametric options, respectively (Ganguli and Ganguly 2016). They test for a significant difference in mean or median, respectively, between two periods (Helsel et al. 2020; Stagge et al. 2014; Ganguli and Ganguly 2016). The Chow (Chow 1960) and Pettitt (Pettitt 1979) tests are other examples of parametric and nonparametric tests, respectively, designed to detect abrupt step differences in the mean of a time series, its magnitude of shifts and changepoints (Mallakpour and Villarini 2016).

These conventional trend analysis methods are simplifications and thus may not capture more complex temporal changes that occur in the real world (Ge et al. 2016). Especially, those methods usually assume a constant long-term drought trend and constant variance, while the true underlying drought trend may be nonlinear under a nonstationary climate, undergo a gradual change in variance/extremes, or both (Pryor et al. 2009; Stagge et al. 2017; Wu et al. 2017). As such, simple linear regression methods cannot capture nonlinear patterns, such as a "pause," acceleration in the rate of change, or abrupt changes. Further, linear trend tests are not designed to capture trends in higher moments, such as variance or skew.

Paired period tests (e.g., the *t* test or Mann–Whitney tests) are sensitive to the selection of two discrete time periods, which can cause inconsistencies across studies using different periods or provide conflicting results (Herweijer et al. 2007; Griffin and Anchukaitis 2014; Ge et al. 2016; Ganguli and Ganguly 2016). For example, Dai (2013) and Sheffield et al. (2012) both studied agricultural/soil moisture drought using PDSI in the United States but provided contradictory long-term trend results. Trenberth et al. (2014) found the choice in base period to be a major cause of this discrepancy. Dai (2013) used a relatively wet base period (1950–79), thereby producing drier trends than Sheffield et al. (2012), which used a longer base period of 1950–2008 (Trenberth et al. 2014).

To expand from a purely temporal analysis to a spatiotemporal analysis of regionally consistent drought trends, studies typically plot the magnitude of conventional trend tests, either displayed as raw values or using isolines (Trenberth et al. 2014). But by relying on a single value for each location to describe the trend, these approaches do not capture more complex, nonlinear patterns like those explored in this study. Cluster analysis is one approach that can be used to identify common patterns among complex data, for example identifying regions with similar patterns of drought or climate (Fovell 1997). Cluster analysis allows the data to drive groupings, rather than predetermining a structure. Fewer studies have used cluster analysis to identify regions with similar patterns of meteorological drought trends (Fovell and Fovell 1993; Haslinger et al. 2019; Mahlstein and Knutti 2010; Sathiaraj et al. 2019) since it is challenging to determine similarity when directly clustering long-time series with large numbers of data points (Distefano et al. 2020). The approach adopted in this study leverages the flexibility of cluster analysis to identify common patterns in parameter estimates from the Non-Stationary Precipitation Index, thereby avoiding the pitfalls of clustering long time series directly.

To address the limitations of linear trend analyses, while also capturing spatiotemporal meteorological drought trends at a regional scale, this study aims 1) to model nonstationary and nonlinear changes in meteorological drought over the twentieth century across the continental United States and 2) to identify subregions with similar dynamics of seasonality and long-term drought trends. To do this, the recently developed Bayesian Non-Stationary Precipitation Index (NSPI) method (Stagge and Sung 2022) is used to simultaneously model the stationary seasonal component of SPI-3 along with gradual nonlinear trends in mean and variance over multiple decades. Instrumental gauges are then clustered based on the fitted NSPI parameters, first based on seasonality and then based on long-term trends. Clustering seasonal parameters is performed to identify climatologically similar stations, similar to previous regionalization studies but with a specific SPI-3 focus, and to validate the results of the NSPI approach. Clustering trends using the long-term NSPI parameters is performed to identify common patterns of century-long climate trends, while retaining the flexibility of nonlinear trends. Using fitted parameters from the NSPI model for clustering reduces the computational burden as well as uncertainty in clustering large sets of data. Further, clustering based on normalized parameter estimates, rather than absolute values, allows for direct comparisons across gauges with widely varied climatology, mimicking the underlying principles of the SPI. Ultimately, this new analysis provides a more flexible and objective spatiotemporal analysis of meteorological drought trends across the United States and is expected to provide insights for regional-scale seasonal precipitation change and to inform future studies of causal mechanisms explaining common patterns of twentieth-century precipitation trends.

2. Method

This study's approach is organized into three sections. First, the NSPI model was fit individually for 656 precipitation gauge records across the continental United States, producing a set of model parameters that describe three interrelated terms: repeating seasonal patterns of NSPI-3, a nonlinear annual trend, and seasonally specific long-term trends. Second, the gauges were clustered according to a subset of fitted model parameters that describe only the recurring seasonal NSPI-3 pattern. Third, the gauges were clustered according to a subset of fitted model parameters that describe only long-term annual trends. Seasonally specific long-term trends were not considered for clustering.

The NSPI approach provides for nonlinear seasonality and long-term precipitation trends, while the clustering approach provides a more objective method to define regions with similar drought trends. The two-step clustering method overcomes the limitation of clustering algorithms in evaluating large datasets having both seasonal and long-term parameters by reducing the parameters used for clustering in each step

(Wang et al. 2013). We expect this two-step clustering (i.e., long-term trends within the same seasonality) to reduce bias produced by larger seasonal variance dominating relatively smaller long-term trend magnitude (Cook et al. 2020).

a. Precipitation data

Daily observed gauge precipitation data (PRCP) were based on the Global Historical Climatology Network dataset at the daily scale (GHCN-D) (Durre et al. 2010). At the time of writing the GHCN-D dataset contains 6542 precipitation gauges in the continental United States. To ensure consistency, we filtered these available records, selecting only gauges where data are available between 1920 and 2018, and at least 80% of the daily data were recorded during this period. A total of 656 gauges across the continental United States satisfied the above criteria and were used to calculate the NSPI based on a 3-month (90-day) accumulation period.

b. Quantify temporal trend: Bayesian NSPI model

We applied the Bayesian Nonstationary SPI model (NSPI; Stagge and Sung 2022) to calculate a nonstationary 3-month SPI-3 wherein the parameters of the gamma distribution can change slowly through time to capture slowly changing precipitation characteristics under climate change (Russo et al. 2013). All fitting was conducted using the "spibayes" package (Stagge 2021). The Bayesian NSPI model allows for nonlinear trends across all distribution parameters using splines (Wood 2004; Marx and Eilers 1998; Wood 2011; Tibshirani et al. 2001) and estimates all daily parameters simultaneously, unlike other nonstationary SPI approaches, which tend to assume linear trends and model each day independently (Stagge and Sung 2022). The NSPI used here is designed to fit the 3-month precipitation using a two-parameter gamma distribution, similarly to a traditional SPI:

$$P_{\text{3months}} \sim \text{Gamma}(\alpha, \theta) \tag{1}$$

where α and θ represent shape and scale parameters, respectively. Seasonality and long-term trends are modeled by setting each parameter of the gamma distribution as a function of time (day and year). Note that this model estimates the mean ($\mu = \alpha\theta$) and shape (α) parameters instead of the shape and scale parameters for more stable estimation. The estimated mean and shape were then used to estimate the scale parameter, $\theta = \mu/\alpha$. The parameters of the gamma distribution were modeled based on the generalized additive modeling (GAM) in terms of day of the year (Julian date), year, and an interaction between Julian date and year. The mean (μ) and shape (α) parameters were therefore estimated using three interaction spline functions, $f(\,)$, for each parameter:

$$E[\log(\mu)] = b_0 + f(x_{\text{Julian\_date}}) + f(x_{\text{year}}) + f(x_{\text{Julian\_date}}, x_{\text{year}}), \tag{2}$$

$$E\left[\frac{1}{\log(\alpha)}\right] = b_0 + f(x_{\text{Julian\_date}}) + f(x_{\text{year}}) + f(x_{\text{Julian\_date}}, x_{\text{year}}), \tag{3}$$

where $f(x_{\text{Julian\_date}})$ represents the seasonal spline by the day of year (Julian date), $f(x_{\text{year}})$ models the change by year, and $f(x_{\text{Julian\_date}}, x_{\text{year}})$ represents long-term trends specific to a given season. This model formulation follows the same approach outlined in greater detail by Stagge and Sung (2022).

Each $f(\,)$ term represents a nonlinear smooth function, or spline, created by summing smooth segments and controlled by regular points called knots (Wood 2004, 2006; Marx and Eilers 1998). The function $f(\,)$ is represented as

$$f(x_i) = \sum_{m=1}^{M} \beta_{im} \mathbf{B}_m x_i, \tag{4}$$

where M is the number of knots, β_{im} is a coefficient that raises or lowers the spline at a given knot m, $\mathbf{B}$ is a model matrix, and x is the location of a point of interest, for example, a given Julian date.

We modeled $f(x_{\text{Julian\_date}})$ as a stationary model with a repeating cyclic spline function for each day of the year. The $f(x_{\text{year}})$ term was a nonstationary, nonrepeating spline, while the $f(x_{\text{Julian\_date}}, x_{\text{year}})$ was modeled as nonstationary tensor interaction product (Stagge and Sung 2022). The tensor spline is useful for modeling the interaction between two variables (Julian date and year), while allowing different smoothness for each dimension. As such, the tensor product spline provides a three-dimensional smooth surface with two axes: Julian date and year. Another strength of the tensor product spline is that the entire tensor surface can be constrained by a few control points' (knots') β_s values. This study used 18 knots for seasonality, spaced every 21 days, and 8 knots for long-term trends to control the spline shape every 14 years. Knots are applied at the same year and Julian date for all gauges to facilitate uniform comparisons.

The β_s control the magnitude of the spline function at each knot and are estimated by Bayesian Monte Carlo Markov chain simulation. Our tensor spline method with normalized parameters is capable of explaining full nonlinear trends using a few parameters at knots both in seasonality and long-term dimensions. Fitting β values can therefore be viewed as a type of dimension reduction prior to clustering. For our clustering purposes, the β_s were standardized to have mean of 0 and standard deviation of 1 at each gauge:

$$\tilde{\beta}_{\text{year},i} = \frac{\beta_{\text{year},i} - \overline{\beta_{\text{year}}}}{\sigma_{\beta_{\text{year}}}}, \tag{5}$$

where $\overline{\beta_{\text{year}}}$ and $\sigma_{\beta_{\text{year}}}$ are the mean and standard deviation of all $\beta_{\text{year},i}$ estimates, respectively, for i knots. This removes differences in absolute value across gauges and allows for a relative comparison. We calculated $\tilde{\beta}_{\text{Julian date}}$ in the same way, normalizing only these seasonal parameters. For clustering and the remainder of this study, we focused only on the mean parameter [Eq. (2)], rather than the shape parameter [Eq. (3)].

c. Cluster analysis

The goal of cluster analysis in this study was to aggregate the observed gauges into clusters with similar patterns of

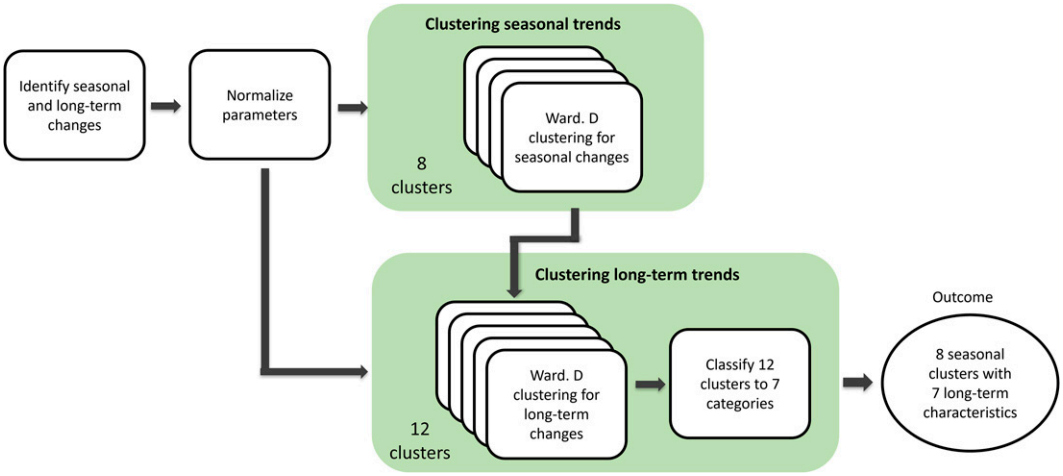

FIG. 1. Framework of clustering analysis.

precipitation seasonality, and then into clusters with similar long-term nonlinear trends. All clustering was conducted via a two-step process: first clustering based on seasonality ($\tilde{\beta}_{\text{Julian\_date}}$) and then clustering within each of these groups based on long-term trends ($\tilde{\beta}_{\text{year}}$) (Fig. 1). Two-step clustering was chosen because seasonal variability, captured with $\tilde{\beta}_{\text{Julian\_date}}$, was much larger than that of interannual trends ($\tilde{\beta}_{\text{year}}$), and thus dominated the clustering. Additionally, seasonality tended to overwhelm interannual trends in clustering because there was more than double the number of β values.

Ward's agglomerative hierarchical clustering method was used to aggregate gauges with similar seasonality and then drought trends. Under Ward's method, cluster distances are defined as the squared Euclidean distances between points and clustering aims to find the group minimizing within-cluster distances (Marston and Ellis 2021; Distefano et al. 2020). The optimal number of clusters for seasonal patterns (clustering 1) and long-term trends (clustering 2) was determined by the gap statistic, comparing the change in within-cluster dispersion with that of a reference null distribution for clustering schemes ranging from 1 to 15 clusters (Tibshirani et al. 2001). A high gap statistic indicates an optimal number of clusters. Gap statistics were calculated via the R package called "factoextra" (Kassambara and Mundt 2020).

3. Results

Here we present the results of meteorological drought clustering performed in two steps, first based on seasonality, and then based on long-term trends using their respective fitted and normalized spline parameters ($\tilde{\beta}_{\text{Julian\_date}}$ and $\tilde{\beta}_{\text{year}}$). This approach clusters regions only based on relative seasonality and long-term trends of the mean parameter instead of its absolute value. In this sense, very dry regions and wet regions could be clustered together if those regions have similar seasonality (clustering 1) or long-term trends (clustering 2).

a. *Seasonal clusters of NSPI-3*

Based on the gap statistic, we retained eight seasonal clusters in clustering 1 using the normalized seasonal betas ($\tilde{\beta}_{\text{Julian\_date}}$), shown spatially (Fig. 2) and seasonally, as a box plot of all $\tilde{\beta}_{\text{Julian\_date}}$ estimates within a cluster (Fig. 3). As can be seen in the combined cluster map in Fig. 2 (lower right corner), seasonally clustered gauges are spatially compact such that most gauges within a seasonal cluster are closely located. It should be noted that the clustering method did not consider location or distance and was based solely on normalized patterns of seasonal precipitation. Where the clusters are not in a single spatial location, they tend to form regionally compact clusters, as in the case of clusters 2, 4, 7, and 8. Clusters are numbered based on their order within the agglomerative clustering dendrogram.

Cluster 6 covers the largest region, occupying most of the middle of the continental United States. It is located throughout many of the central plains states, which have dry winters and a wet seasonal peak during summer (Fig. 3). Seasonality varies little within this cluster, as indicated by relatively small variance despite the large number of stations (Fig. 3; cluster 6). In the eastern part of the United States, cluster 5 represents a narrow transitional band between the central plains states (cluster 6) and the southeastern United States (cluster 2) near the Mississippi and Ohio Rivers. As a transitional region, cluster 5's seasonality is similar to these two neighboring clusters (Fig. 3). Clusters 5 and 6 both have dry winters and wet summers; however, cluster 5 has a longer dry period, lasting from September to the end of April, similar to its southeastern neighbor (cluster 2). In this way cluster 5 represents a transition between the climate of cluster 6 (the Great Plains states) and cluster 2 (the Southeast), which agrees with its geographic location (Fig. 2). Gauges of cluster 8 are located along the outer edges of cluster 6, separated into distinct regions to the northeast (Great Lakes and New England) and south/southwest. The seasonality of cluster 8 is similar to that of cluster 6 (Fig. 3) but shows less difference between wet and dry seasons, with its wet period occurring later during fall than cluster 6.

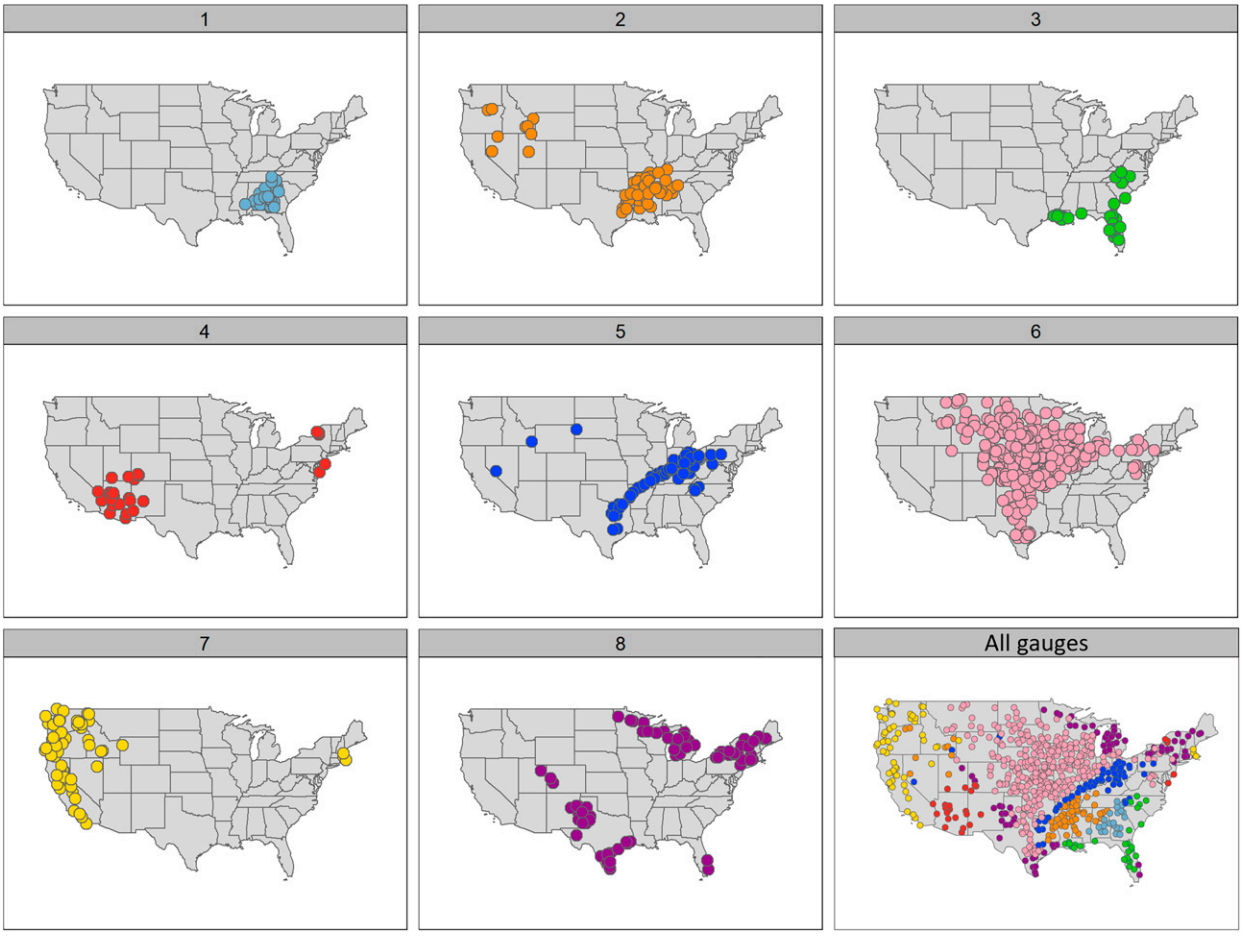

FIG. 2. Spatial patterns of clusters based on seasonal patterns of the precipitation distribution mean. Each cluster is shown in a separate panel for clarity and combined in the final panel with colors corresponding to cluster.

The southeastern United States was divided into three clusters (clusters 1–3). Cluster 3 is predominantly coastal, while clusters 1 and 2 separate the southeast into more eastern and western subregions, respectively (Fig. 2). Cluster 2 has a similar spring/summer wet peak and late summer dry period as its neighbor, cluster 5, but with a more consistent wet period (Fig. 3). Referring to Fig. 3, cluster 1 has two wet seasons, one in late March to the beginning of April and another at the end of July, with the dry period occurring in winter around November to December. Cluster 3 is seasonally reversed, with the wettest season occurring in the fall and driest season in the winter and spring. This unique seasonality is likely related to cluster 3's coastal influence.

Cluster 4 (the desert Southwest) has two wet periods, February–April and September–October, separated by a dry period during summer (Fig. 3). It is important to note here that because the SPI-3 is a backward looking 3-month precipitation metric, the mean parameter for March 1 measures total precipitation from the previous 1 December through 1 March, or the classical DJF winter period. The Southwest cluster 4 shows noticeably large variance among the gauges. This is because the mean parameter (μ) values are very small in the semiarid southwest (near zero), such that the normalizing via $\tilde{\beta}_{\text{Julian\_date}}$ accentuates what are actually very small differences in absolute value. There are a few gauges in the mid-Atlantic coast (cluster 4) that follow a similar bimodal seasonality to the Southwest, despite having a very different total precipitation (Fig. 2). The West coast region (cluster 7) has a unique seasonality compared to other regions. Unlike most other regions, cluster 7 has a short wet season during winter and a clear dry period over summer and fall (Fig. 3).

b. *Long-term precipitation trend clusters*

In clustering step 2, we retained 12 long-term clusters within each of the eight seasonal clusters, although the cluster analyses were performed independently for each region identified in clustering step 1. This second clustering was based on the extracted $\tilde{\beta}_{\text{year}}$ parameters from the model [Eq. (2)] for each gauge. This produced a total of 96 unique clusters combining seasonality and long-term trend parameters. Although we calculated the gap statistic to determine the optimal number of long-term clusters under each seasonal clusters, 12 clusters was a common solution to all regions and so was applied throughout to maintain consistency. The two-step clustering

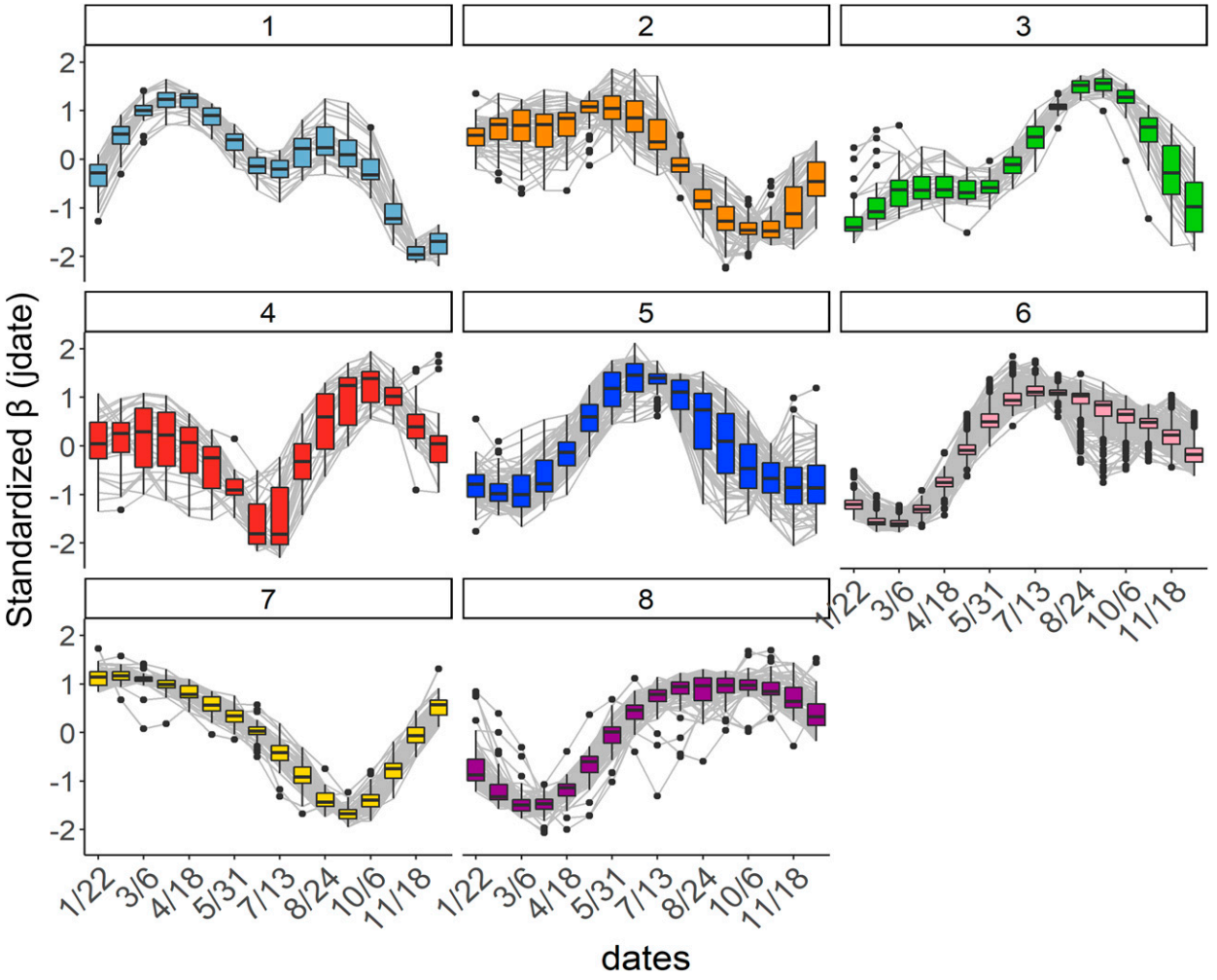

FIG. 3. Mean parameters of all gauges under same seasonal clusters in terms of Julian date. Cluster numbers and colors match those in Fig. 2.

process helps to isolate parameters of seasonality and long-term trend by preventing large variance from mixing many numbers of variables with different scales.

Despite the consistent finding of 12 long-term clusters within each region, when viewed qualitatively, we concluded that these 12 long-term clusters fall under seven more general patterns. We therefore categorized each based on the relative pattern of $\tilde{\beta}_{\text{year}}$ during the observed period. In order from wetting to drying, these patterns are increasingly wetter (W), drier and then wetter (DW), wetter–drier–wetter (WDW), drier–wetter–drier (DWD), wetter–drier (WD), increasingly drier (D), and no trends (NA). The classification is determined based on the direction of change and the number of sign changes in the set of during the observed period. This manual classification rule was then applied across all seasonal clusters to recategorize each long-term cluster into seven more general long-term patterns (Fig. 4). All spatial comparisons are based on these seven long-term patterns. Figure 4 shows typical examples of these temporal patterns, ranging from continuously drier or wetter (left; D, W), to midcentury reversals (center; WD, DW) and multidecadal fluctuations (right; DWD, WDW). The seventh pattern is NA, representing patterns that are hard to define or do not have enough gauges to demonstrate a pattern. They are not shown here.

The spatial patterns of long-term precipitation trends are shown in Fig. 5. The color scale is based on whether modern precipitation is drier (red) or wetter (blue) presently than in the past. Midcentury reversals (WD or DW) are colored as intermediate patterns, while the DWD and WDW patterns show little long-term trend and instead display multidecadal cycles. Spatial patterns of long-term trend are not homogenously organized by seasonal cluster. Instead, each seasonally based cluster has mixed types of long-term trends.

Although long-term precipitation patterns do not strictly follow the climate regions established via seasonal clustering, there are emergent patterns when viewed across the contiguous United States (Figs. 5 and 6). Overall, these results capture a dominant wetter trend in the north and eastern parts of the United States and a dominant drier trend in the western United States throughout the twentieth century. This trend is clearer when we exclude relatively weak cyclic signals (WDW and DWD) and focus on either continuous increase/decrease

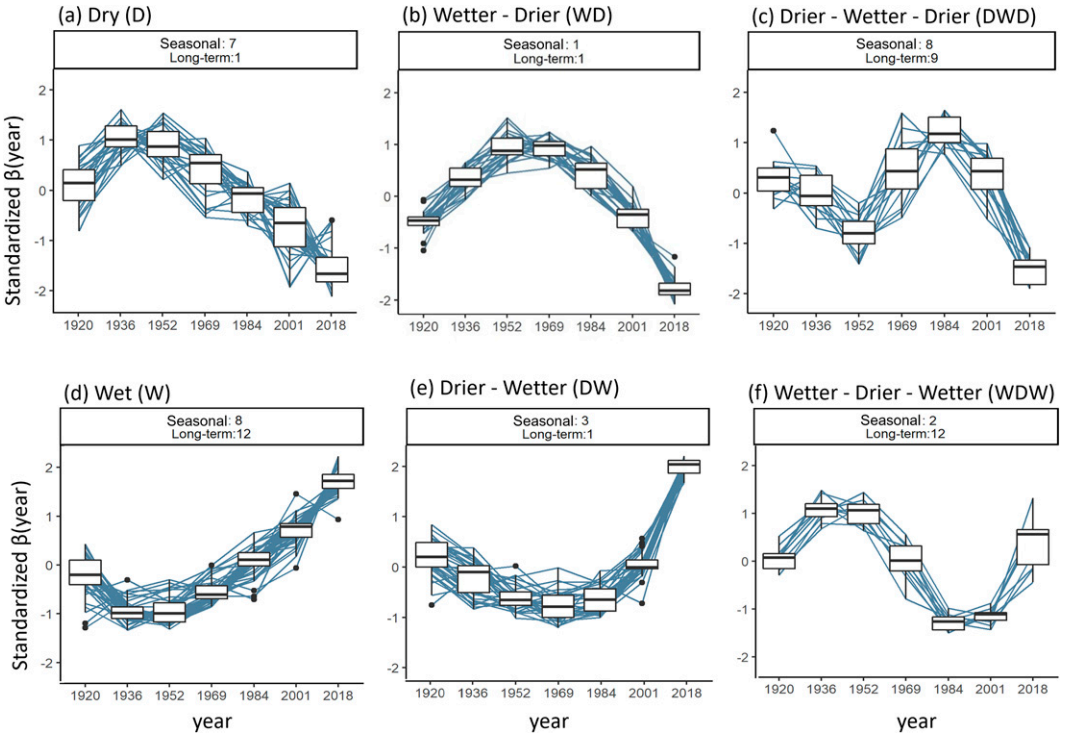

FIG. 4. Example of six categories of long-term trends. "Seasonal" means seasonal clusters and "long-term" means the long-term clusters.

(D, W) or long-term trends with a midcentury pause or reversal (DW, WD) in Fig. 6. This highlights the significant wetting trend across the northern central United States and the Midwest and the drying trend in the western United States during the last century.

The progressively drier patterns in the west and southwest regions are primarily captured by clusters 4 and 7 (Fig. 5). Cluster 6, which covers much of the center of the United States, has mixed trends because of its large area (Fig. 5). However, wetter trends are more noticeable in the northern portion while drier trends are dominant in the southern portion. This is accentuated when only the strong trends are retained (Fig. 6). The majority of the central United States in cluster 6 underwent a DW pattern, with an extended dry period in the midcentury (1930–50), followed by a steady wetting period (Fig. 4). The most northern portions of cluster 6 do not demonstrate this midcentury reversal, instead showing a steadier wetting pattern (Fig. 6).

By excluding weaker patterns with little long-term trends, the wetting trend previously shown in Florida (Fig. 5, cluster 3) was removed (Fig. 6), as this region only has WDW trends. This indicates that the long-term precipitation trends in Florida are not very significant but rather follow a more cyclic pattern with little long-term change. Excluding DWD patterns also provides a clearer spatial pattern in the southern plains states compared to Fig. 5. The wetting trend that occupies much of the northern plains states extends into Oklahoma and continues into northern Texas before transitioning to a moderate drying trend in central and southern Texas. We note that the long-term trend in Kansas shows mixed spatial patterns of both drying and wetting trends, likely due to its location at the conjunction of the drying west and wetter north.

4. Discussion

Our study answers the question "What are the spatial patterns of meteorological drought in continental United States when non-stationary and non-linear changes are considered?" Using the normalized mean parameters from the NSPI purposefully removes the dramatic differences in precipitation magnitude across the United States to permit a clearer focus on common seasonal patterns and relative change in precipitation over time. For example, this approach can highlight gauges with similar timing of annual wet/dry seasons and highlight differences between gauges where annual precipitation has steadily increased during the last century and those gauges where increases only occurred following a midcentury low. Use of a normalized, rather than absolute magnitude, comparison mimics the basic principles of the normalized SPI, which evaluates drought severity in terms of a relative anomaly for a given climate. Here we discuss common and distinctive features of our seasonal and long-term trend findings relative to existing studies to highlight their importance.

a. Spatial patterns in seasonality

Defining subregions by similar drought characteristics and setting up water management plans based on climate rather than the political boundaries can be valuable in managing

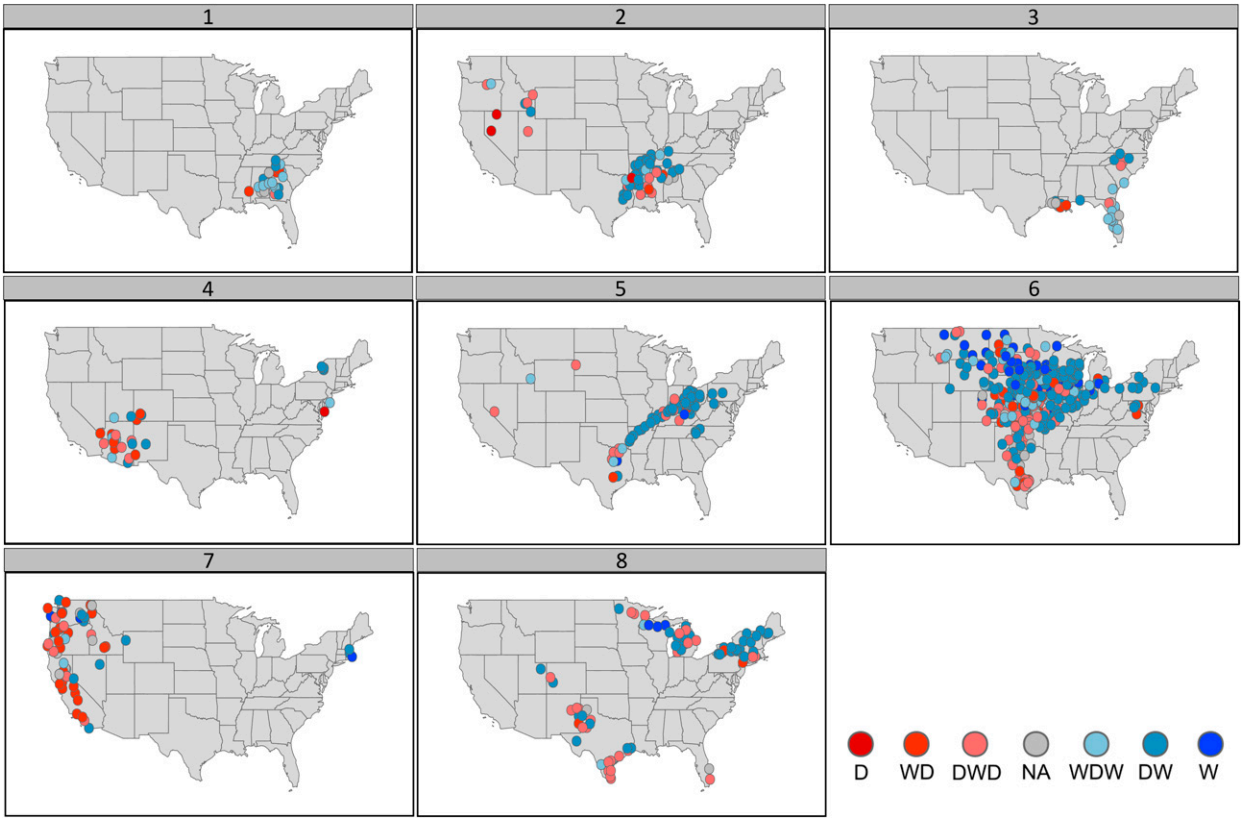

FIG. 5. Long-term trends in each seasonal cluster. Seasonal clusters are separated into subfigures, while the color represents the general direction of change for the seven long-term patterns.

drought risk (Coopersmith et al. 2014). The seasonal cluster approach (section 3a) provides insight into characterizing regions with similar precipitation seasonality by aggregating gauges based on the seasonal term from the 3-month NSPI model. The seasonal clusters identified here generally agree with previous regionalization schemes; however, the specific focus on 3-month precipitation provides some greater insights that could be more useful for meteorological drought monitoring or water resources planning.

We found that the seasonal clusters derived using our approach (Figs. 2 and 3) were mostly dictated by seasonal periods of greatest precipitation, rather than dry seasons.

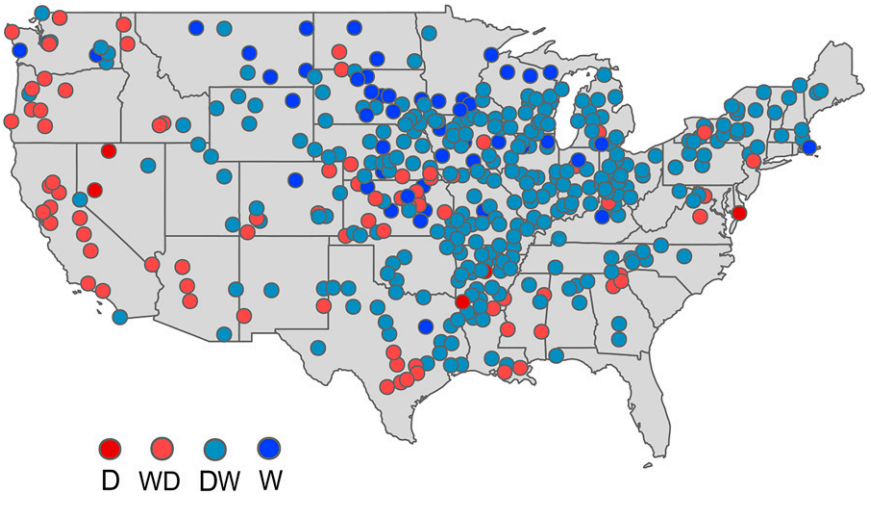

FIG. 6. Long-term trends in the continental United States.

Therefore, the prevailing atmospheric circulation patterns that drive wetter seasons play a large role in determining the distinctive seasonality of each cluster. For example, cluster 3 in the coastal Southeast including the Gulf of Mexico and Florida (Figs. 2 and 3) appears to be controlled by hurricane and tropical storm peaks bringing large precipitation during the summer (Brun and Barros 2014), as indicated by a peak in late August (Fig. 3). Atmospheric drivers also define cluster 4 in the Southwest, which is dominated by the effect of the summer monsoon (Fig. 3). The spatial extent of cluster 4 matches prior studies of this monsoon affected region (Hu and Feng 2008).

Seasonal clusters also appear to be highly dependent on topography. For example, the central cluster 6 is a large, homogenous region. As one would expect, the topography of this region is also quite homogenous with relatively few topographic extremes. This is contrasted with the west coast (cluster 7), which is generally bounded to its east by the Sierra Nevada Mountains to the south and the Cascade mountain range to the north. The region of greatest topographic complexity, the Rocky Mountains, is not captured by a single seasonal cluster (Fig. 2), likely due to this complexity. This complex precipitation seasonality in the Rocky Mountains coincides with the previous study of revised Köppen–Geiger climate classification, which shows complex temperature and precipitation patterns throughout this mountainous region (Beck et al. 2018).

Some regions in this study (Fig. 2) agree well with Köppen–Geiger climate regions, which groups global climate into 30 classes based on absolute mean seasonal temperature and precipitation patterns (Beck et al. 2018). Similar to our findings, the Köppen–Geiger classification divides California and Arizona into separate regions despite their close spatial distance (Fig. 2). The Köppen–Geiger scheme also considers the Great Lakes region and southern Florida (cluster 8) distinct from their respective surroundings, although these areas are combined in our study due to precipitation seasonality (Fig. 4) but separated in Köppen–Geiger because of its consideration of temperature. This discontinuous grouping (cluster 8) is supported by Marston and Ellis (2021) showing both regions with a wet fall and dry spring.

The differences between the seasonal clusters identified here and the Köppen–Geiger can be attributed to our focus solely on normalized NSPI-3 whereas the Köppen–Geiger also considers absolute precipitation and temperature. Our study subdivides precipitation seasonality in the eastern United States into much greater detail (five clusters) than the Köppen–Geiger, which divides the same region into two parts: north and south (Seager et al. 2019). As mentioned, the southeast region in this study was subdivided because their peak precipitation seasons vary from early spring to late fall (clusters 1, 2, and 5) (Fig. 4). In addition, our results do not show the typical 100th meridian division, which bisects the United States into the arid western and humid eastern regions in many studies including the Köppen–Geiger scheme (Coopersmith et al. 2014; Beck et al. 2018; Hu and Feng 2008). Rather, cluster 6 (Fig. 2) covers most of the Great Plains in the central United States, spanning this dividing line. The lack of the 100th meridian in our study stems from our focus solely on relative precipitation seasonality, which is similar throughout this entire region, rather than absolute precipitation or consideration of temperature as in Köppen–Geiger methods (Seager et al. 2019).

Our results emphasize the improved regional boundaries in observing seasonality in meteorological drought. In this way, the seasonal clusters developed here support and confirm existing climatic regions defined by National Centers for Environmental Information (NCEI) or Köppen–Geiger, while also providing greater nuance and a specific focus on precipitation seasonality, irrespective of temperature or annual absolute precipitation (Marvel et al. 2021; Marston and Ellis 2021).

Our new regional boundaries contribute to improving water management plans by identifying the region with the season when water is relatively abundant or deficit (Dalton et al. 2013). For example, a reservoir operation plan—when to release or store water—can be adopted based on other regions in the cluster as it is highly affected by seasonality of precipitation. Our clusters can also be an important determinant to manage agricultural productivity (Guido et al. 2020). Existing studies that define the region with absolute seasonal precipitation have a limitation in investigating this variability since those classifications are highly driven by general wet and dry climate; they aggregated the entire eastern United States to the same cluster whereas our study captures detailed wet and dry periods (Beck et al. 2017; Tallaksen and van Lanen 2004).

b. Regional patterns of long-term precipitation trends

The results of this study generally corroborate previous studies that found increasingly wetter conditions in the east and drier conditions in the western United States (Slater et al. 2021; Ganguli and Ganguly 2016). However, while our results broadly agree with prior studies of precipitation change over the instrumental period, some results differ from those using only linear trend analysis. For example, Ganguli and Ganguly (2016) compared the long-term trend of SPI between the periods 1926–69 and 1970–2013 and found a clear drier trend in California and wetter trend in Florida. While agreeing in California, the wetter trend in Florida is less significant or negligible in our results. The discrepancy can be attributed to our study evaluating trend based on the full period while the previous study compares two averaged periods. Findings for the central portion of the United States (cluster 6) further highlight the importance of considering nonlinear trends. There is a north–south gradient ranging from a constant wetting pattern (W) in the upper Mississippi River valley (northern cluster 6) to a wetting pattern with a midcentury low in the central Mississippi Valley (central cluster 6 and cluster 5), and ultimately mixed patterns in the southern portions of cluster 6. In particular, the midcentury low corresponds to the major droughts of the 1930s and 1950s (Heim 2017). The severe drought of 1954 affected this region south of 40°N, approximately at the breakpoint between the W patterns to the north and the DW patterns to the south (Fig. 6). A linear analysis of the DW region may have found only a mild wetting

or negligible trend in this region, whereas this study identifies several exceptionally dry decades in the mid-twentieth century followed by a strong wetting trend toward more precipitation than the earliest records.

The Kansas region, located in the center of the United States, is at the confluence of the east–west wet–dry pattern and the north–south gradient within cluster 6. This region thereby produced a complex mix of long-term trend patterns (Figs. 5 and 6). Previous studies have found similar conflicting trend results for this region (Rahmani et al. 2015; Anandhi et al. 2016). Rahmani et al. (2015) pointed out that change patterns in observed precipitation records in the Kansas area are not coherent, and only some of the precipitation records show a statistically significant increasing trend. By incorporating nonlinear trends and clustering across the continental United States, this study places prior conflicting results in Kansas into a clearer spatial context, located at the center of several competing trends.

Another example highlighting the value of combining NSPI nonlinear trends with clustering was found in the Southeast. Mitra and Srivastava (2016) suggest that the southeastern United States, except for Florida, experienced drier conditions during 1936–70 and wetter conditions (less frequent drought) during 1970–2005. This would be equivalent to either a wetting (W) or midcentury reversal (DW) in the trend classification system established here. However, our study showed more complex spatial patterns, with the more western subregions of Louisiana and Mississippi (cluster 2) experiencing drier trends (WD, DWD) while the more eastern states of Alabama and Georgia (cluster 1) have undergone a wetter trend (DW, WDW). This discrepancy is likely caused by the prior study's comparison of two discrete periods, rather than capturing the full shape of trends, as performed here. Defining the long-term change of the region with a nonlinear trend or pattern such as wetter–drier helps us understand historical dry and wet periods and ultimately better prepare for the decadal scale of cyclic wet and dry conditions.

We also note that several regions appear to have experienced abrupt changes or acceleration of trends after the year 2000. For example, the long-term change patterns (DWD, DW, and WDW) shown in Figs. 4c, 4e, and 4f each have abrupt or dramatic changes during the last decade (2001–18). Splines can be unduly influenced by so-called edge effects, emphasizing extreme values at the beginning or end of a series, but this finding warrants future detailed investigation of these regions. Detecting regions having those abrupt changes in WDW or DWD patterns helps to identify recent trend changes in some regions. This overcomes the limitation of comparing averaged two time periods, which tends to dilute the level of very recent shifts in drought severity and catch the up-to-date drought trend interrelated to climate change.

5. Conclusions

This study investigated spatiotemporal meteorological drought trends using a novel approach: NSPI modeling for temporal trends among the SPI distribution parameters and a two-step clustering approach to categorize seasonality and common long-term patterns. NSPI modeling captured complex nonlinear trends such as direction changes or cyclic variability and represents these patterns using few parameters. The NSPI modeling approach also benefited from analyzing seasonality and long-term trends in a single model, decreasing uncertainty by greatly increasing the number of data points.

Separating the NSPI parameters into two components (seasonality and long-term trend) permitted two-step clustering. The two-step clustering approach avoids bias caused by scale differences between seasonal and long-term parameters. By categorizing gradual precipitation trends across the United States into a few patterns, it simplifies interpretation of the nonlinear trends while better capturing more complex patterns beyond simple linear increases and decreases. Benefits for this were shown particularly in the central United States where the approach distinguished between continuous long-term precipitation increases in the north and an increase in the central latitudes that was interrupted by a multidecadal period of drought in the 1930s to the 1950s. It further highlighted intensifications and changes that have occurred in the last decades, which otherwise would have been ignored in a linear regression.

Our study corroborates results showing that the general meteorological drought trends of a wetter eastern and a drier western United States can be more complex at the local scale (Orlowsky and Seneviratne 2013; Marvel et al. 2021; Ganguli and Ganguly 2016). In addition, we found that long-term precipitation trends (Fig. 5) are less spatially coherent than seasonality (Fig. 2) and do not follow seasonally based regions. We further found several unique features not previously emphasized, such as a north–south gradient in the central United States and a more complex pattern in the Southeast, which changes from drier trends near the Mississippi River to wetter trends near the Atlantic coast. These regionally specific trend findings can inform future causal studies investigating local-scale long-term drought trends interrelated to global and local climate (Dai 2011).

We recommend future studies focus on nonlinear trends in the shape parameter. The shape parameters control variance and the extreme tails of the distribution. This study focused solely on the mean, but the NSPI methodology simultaneously produces shape parameter estimates. In addition, identifying shifts in seasonality is important, since these seasonal shifts could impact existing water management schemes, with annual precipitation remaining constant (i.e., no detectable trend) (Slater et al. 2021). Thus, research is also needed to address shifts in seasonality or seasonally specific long-term trends, as measured by the interaction term in our model. Preliminary investigation of the interaction term showed more complex patterns, which would require more detailed study. We therefore recommend further study of seasonal trends at the regional or local scale, where underlying causal mechanisms can be better explored. Further study is also needed to explore how the observed trends during the last century link with projections of the future climate. Analyzing trends using climate projection poses a new set of challenges because the model would have to account for different carbon emission scenarios and multiple models, each with their own specific

bias. The GAM model presented here provides a potential to incorporate future trends, but would require further development.

Ultimately this study provides better insight into understanding gradual drought changes, especially distinguishing monotonic increase or decrease from cyclic wetter and drier conditions or recent abrupt changes. Our results will contribute to highlighting vulnerable regions that have experienced drier trends. Understanding local-scale drought trends can ultimately improve planning of community-scale water resources management (Marvel et al. 2021).

Acknowledgments. This work was supported primarily by the Paleo Perspectives on Climate Change (P2C2) Program of the National Science Foundation under NSF Project 2002539 ("Leveraging Bayesian approaches to link reconstructed, observed, and projected meteorological drought while accounting for inherent data biases"). Any opinions, findings, and conclusions or recommendations expressed in this material are those of the author(s) and do not necessarily reflect those of the National Science Foundation. The work was also supported by the Byrd Polar and Climate Research Center at the Ohio State University.

Data availability statement. All code, data, and instructions are available via an open access repository at https://doi.org/10.5281/zenodo.5832030.

REFERENCES

Anandhi, A., S. Hutchinson, J. Harrington, V. Rahmani, M. B. Kirkham, and C. W. Rice, 2016: Changes in spatial and temporal trends in wet, dry, warm and cold spell length or duration indices in Kansas, USA. *Int. J. Climatol.*, **36**, 4085–4101, https://doi.org/10.1002/joc.4619.

Andreadis, K. M., and D. P. Lettenmaier, 2006: Trends in 20th century drought over the continental United States. *Geophys. Res. Lett.*, **33**, L10403, https://doi.org/10.1029/2006GL025711.

Beck, H. E., A. I. J. M. van Dijk, V. Levizzani, J. Schellekens, D. G. Miralles, B. Martens, and A. de Roo, 2017: MSWEP: 3-hourly 0.25° global gridded precipitation (1979–2015) by merging gauge, satellite, and reanalysis data. *Hydrol. Earth Syst. Sci.*, **21**, 589–615, https://doi.org/10.5194/hess-21-589-2017.

——, N. E. Zimmermann, T. R. McVicar, N. Vergopolan, A. Berg, and E. F. Wood, 2018: Present and future Köppen-Geiger climate classification maps at 1-km resolution. *Sci. Data*, **5**, 180214, https://doi.org/10.1038/sdata.2018.214.

Brun, J., and A. P. Barros, 2014: Mapping the role of tropical cyclones on the hydroclimate of the southeast United States: 2002–2011. *Int. J. Climatol.*, **34**, 494–517, https://doi.org/10.1002/joc.3703.

Byrne, M. P., and P. A. O'Gorman, 2015: The response of precipitation minus evapotranspiration to climate warming: Why the "wet-get-wetter, dry-get-drier" scaling does not hold over land. *J. Climate*, **28**, 8078–8092, https://doi.org/10.1175/JCLI-D-15-0369.1.

Chou, C., J. C. H. Chiang, C.-W. Lan, C.-H. Chung, Y.-C. Liao, and C.-J. Lee, 2013: Increase in the range between wet and dry season precipitation. *Nat. Geosci.*, **6**, 263–267, https://doi.org/10.1038/ngeo1744.

Chow, G. C., 1960: Tests of equality between sets of coefficients in two linear regressions. *Econometrica*, **28**, 591–605, https://doi.org/10.2307/1910133.

Cook, B. I., T. R. Ault, and J. E. Smerdon, 2015: Unprecedented 21st century drought risk in the American Southwest and Central Plains. *Sci. Adv.*, **1**, e1400082, https://doi.org/10.1126/sciadv.1400082.

——, R. Seager, A. P. Williams, M. J. Puma, S. McDermid, M. Kelley, and L. Nazarenko, 2019: Climate change amplification of natural drought variability: The historic mid-twentieth-century North American drought in a warmer world. *J. Climate*, **32**, 5417–5436, https://doi.org/10.1175/JCLI-D-18-0832.1.

——, J. S. Mankin, K. Marvel, A. P. Williams, J. E. Smerdon, and K. J. Anchukaitis, 2020: Twenty-first century drought projections in the CMIP6 forcing scenarios. *Earths Future*, **8**, e2019EF001461, https://doi.org/10.1029/2019EF001461.

Cook, E. R., R. Seager, R. R. Heim, R. S. Vose, C. Herweijer, and C. Woodhouse, 2010: Megadroughts in North America: Placing IPCC projections of hydroclimatic change in a long-term palaeoclimate context. *J. Quat. Sci.*, **25**, 48–61, https://doi.org/10.1002/jqs.1303.

Coopersmith, E. J., B. S. Minsker, and M. Sivapalan, 2014: Patterns of regional hydroclimatic shifts: An analysis of changing hydrologic regimes. *Water Resour. Res.*, **50**, 1960–1983, https://doi.org/10.1002/2012WR013320.

Dai, A., 2011: Drought under global warming: A review. *Wiley Interdiscip. Rev.: Climate. Change*, **2**, 45–65, https://doi.org/10.1002/wcc.81.

——, 2013: Increasing drought under global warming in observations and models. *Nat. Climate Change*, **3**, 52–58, https://doi.org/10.1038/nclimate1633.

——, T. Zhao, and J. Chen, 2018: Climate change and drought: A precipitation and evaporation perspective. *Curr. Climate. Change Rep.*, **4**, 301–312, https://doi.org/10.1007/s40641-018-0101-6.

Dalton, M., P. Mote, and A. Snover, 2013: *Climate Change in the Northwest: Implications for our Landscapes, Waters, and Communities*. Island Press, 271 pp., https://cig.uw.edu/publications/climate-change-in-the-northwest-implications-for-our-landscapes-waters-and-communities/.

Diffenbaugh, N. S., 2020: Verification of extreme event attribution: Using out-of-sample observations to assess changes in probabilities of unprecedented events. *Sci. Adv.*, **6**, eaay2368, https://doi.org/10.1126/sciadv.aay2368.

Distefano, V., V. Mameli, and I. Poli, 2020: Identifying spatial patterns with the Bootstrap ClustGeo technique. *Spat. Stat.*, **38**, 100441, https://doi.org/10.1016/j.spasta.2020.100441.

Durre, I., M. J. Menne, B. E. Gleason, T. G. Houston, and R. S. Vose, 2010: Comprehensive automated quality assurance of daily surface observations. *J. Appl. Meteor. Climatol.*, **49**, 1615–1633, https://doi.org/10.1175/2010JAMC2375.1.

Fovell, R. G., 1997: Consensus clustering of U.S. temperature and precipitation data. *J. Climate*, **10**, 1405–1427, https://doi.org/10.1175/1520-0442(1997)010<1405:CCOUST>2.0.CO;2.

——, and M.-Y. C. Fovell, 1993: Climate zones of the conterminous United States defined using cluster analysis. *J. Climate*, **6**, 2103–2135, https://doi.org/10.1175/1520-0442(1993)006<2103:CZOTCU>2.0.CO;2.

Ganguli, P., and A. R. Ganguly, 2016: Space–time trends in U.S. meteorological droughts. *J. Hydrol. Reg. Stud.*, **8**, 235–259, https://doi.org/10.1016/j.ejrh.2016.09.004.

Ge, Y., T. Apurv, and X. Cai, 2016: Spatial and temporal patterns of drought in the continental U.S. during the past century. *Geophys. Res. Lett.*, **43**, 6294–6303, https://doi.org/10.1002/2016GL069660.

Griffin, D., and K. J. Anchukaitis, 2014: How unusual is the 2012–2014 California drought? *Geophys. Res. Lett.*, **41**, 9017–9023, https://doi.org/10.1002/2014GL062433.

Guido, Z., and Coauthors, 2020: Farmer forecasts: Impacts of seasonal rainfall expectations on agricultural decision-making in sub-Saharan Africa. *Climate. Risk Manage.*, **30**, 100247, https://doi.org/10.1016/j.crm.2020.100247.

Guttman, N. B., 1999: Accepting the standardized precipitation index: A calculation algorithm. *J. Amer. Water Resour. Assoc.*, **35**, 311–322, https://doi.org/10.1111/j.1752-1688.1999.tb03592.x.

Haslinger, K., F. Holawe, and G. Blöschl, 2019: Spatial characteristics of precipitation shortfalls in the Greater Alpine Region—A data-based analysis from observations. *Theor. Appl. Climatol.*, **136**, 717–731, https://doi.org/10.1007/s00704-018-2506-5.

Heim, R. R., 2002: A review of twentieth-century drought indices used in the United States. *Bull. Amer. Meteor. Soc.*, **83**, 1149–1166, https://doi.org/10.1175/1520-0477-83.8.1149.

——, 2017: A comparison of the early twenty-first century drought in the United States to the 1930s and 1950s drought episodes. *Bull. Amer. Meteor. Soc.*, **98**, 2579–2592, https://doi.org/10.1175/BAMS-D-16-0080.1.

Helsel, D. R., R. M. Hirsch, K. R. Ryberg, S. Archfield, and E. J. Gilroy, 2020: Statistical methods in water resources: Techniques and methods 4-A3. U.S. Geological Survey, accessed 4 August 2021, https://doi.org/10.3133/tm4A3.

Herweijer, C., R. Seager, E. R. Cook, and J. Emile-Geay, 2007: North American droughts of the last millennium from a gridded network of tree-ring data. *J. Climate*, **20**, 1353–1376, https://doi.org/10.1175/JCLI4042.1.

Hoerling, M., J. Eischeid, J. Perlwitz, X. Quan, T. Zhang, and P. Pegion, 2012: On the increased frequency of Mediterranean drought. *J. Climate*, **25**, 2146–2161, https://doi.org/10.1175/JCLI-D-11-00296.1.

Hu, Q., and S. Feng, 2008: Variation of the North American summer monsoon regimes and the Atlantic multidecadal oscillation. *J. Climate*, **21**, 2371–2383, https://doi.org/10.1175/2007JCLI2005.1.

Hu, Z., X. Chen, D. Chen, J. Li, S. Wang, Q. Zhou, G. Yin, and M. Guo, 2019: "Dry gets drier, wet gets wetter": A case study over the arid regions of central Asia. *Int. J. Climatol.*, **39**, 1072–1091, https://doi.org/10.1002/joc.5863.

Kassambara, A., and F. Mundt, 2020: factoextra: Extract and visualize the results of multivariate data analyses. R package version 1.0.7, https://rdrr.io/cran/factoextra/.

Lee, J., D. Waliser, H. Lee, P. Loikith, and K. E. Kunkel, 2019: Evaluation of CMIP5 ability to reproduce twentieth century regional trends in surface air temperature and precipitation over conus. *Climate Dyn.*, **53**, 5459–5480, https://doi.org/10.1007/s00382-019-04875-1.

Lloyd-Hughes, B., 2014: The impracticality of a universal drought definition. *Theor. Appl. Climatol.*, **117**, 607–611, https://doi.org/10.1007/s00704-013-1025-7.

——, and M. A. Saunders, 2002: A drought climatology for Europe. *Int. J. Climatol.*, **22**, 1571–1592, https://doi.org/10.1002/joc.846.

Mahlstein, I., and R. Knutti, 2010: Regional climate change patterns identified by cluster analysis. *Climate Dyn.*, **35**, 587–600, https://doi.org/10.1007/s00382-009-0654-0.

Mallakpour, I., and G. Villarini, 2016: A simulation study to examine the sensitivity of the Pettitt test to detect abrupt changes in mean. *Hydrol. Sci. J.*, **61**, 245–254, https://doi.org/10.1080/02626667.2015.1008482.

Mann, H. B., 1945: Nonparametric tests against trend. *Econometrica*, **13**, 245–259, https://doi.org/10.2307/1907187.

Marston, M. L., and A. W. Ellis, 2021: Delineating precipitation regions of the contiguous United States from cluster analyzed gridded data. *Ann. Amer. Assoc. Geogr.*, **111**, 1721–1739, https://doi.org/10.1080/24694452.2020.1828803.

Marvel, K., B. I. Cook, C. Bonfils, J. E. Smerdon, A. P. Williams, and H. Liu, 2021: Projected changes to hydroclimate seasonality in the continental United States. *Earth's Future*, **9**, e2021EF002019, https://doi.org/10.1029/2021EF002019.

Marx, B. D., and P. H. C. Eilers, 1998: Direct generalized additive modeling with penalized likelihood. *Comput. Stat. Data Anal.*, **28**, 193–209, https://doi.org/10.1016/S0167-9473(98)00033-4.

McKee, T. B., N. J. Doesken, and J. Kleist, 1993: The relationship of drought frequency and duration to time scales. *Eighth Conf. on Applied Climatology*, Anaheim, CA, Amer. Meteor. Soc., 179–184.

Mishra, A. K., and V. P. Singh, 2010: A review of drought concepts. *J. Hydrol.*, **391**, 202–216, https://doi.org/10.1016/j.jhydrol.2010.07.012.

Mitra, S., and P. Srivastava, 2016: Spatiotemporal variability of meteorological droughts in southeastern USA. *Nat. Hazards*, **86**, 1007–1038, https://doi.org/10.1007/s11069-016-2728-8.

Orlowsky, B., and S. I. Seneviratne, 2013: Elusive drought: Uncertainty in observed trends and short- and long-term CMIP5 projections. *Hydrol. Earth Syst. Sci.*, **17**, 1765–1781, https://doi.org/10.5194/hess-17-1765-2013.

Palmer, W. C., 1965: *Meteorological Drought.* U.S. Department of Commerce, Weather Bureau, 68 pp.

Pettitt, A. N., 1979: A non-parametric approach to the change-point problem. *J. Roy. Stat. Soc.*, **28C**, 126–135, https://doi.org/10.2307/2346729.

Pryor, S. C., J. A. Howe, and K. E. Kunkel, 2009: How spatially coherent and statistically robust are temporal changes in extreme precipitation in the contiguous USA? *Int. J. Climatol.*, **29**, 31–45, https://doi.org/10.1002/joc.1696.

Rahmani, V., S. L. Hutchinson, J. A. H. Jr, J. M. S. Hutchinson, and A. Anandhi, 2015: Analysis of temporal and spatial distribution and change-points for annual precipitation in Kansas, USA. *Int. J. Climatol.*, **35**, 3879–3887, https://doi.org/10.1002/joc.4252.

Russo, S., A. Dosio, A. Sterl, P. Barbosa, and J. Vogt, 2013: Projection of occurrence of extreme dry-wet years and seasons in Europe with stationary and nonstationary standardized precipitation indices. *J. Geophys. Res. Atmos.*, **118**, 7628–7639, https://doi.org/10.1002/jgrd.50571.

Sathiaraj, D., X. Huang, and J. Chen, 2019: Predicting climate types for the continental United States using unsupervised clustering techniques. *Environmetrics*, **30**, e2524, https://doi.org/10.1002/env.2524.

Seager, R., A. Tzanova, and J. Nakamura, 2009: Drought in the southeastern United States: Causes, variability over the last millennium, and the potential for future hydroclimate change. *J. Climate*, **22**, 5021–5045, https://doi.org/10.1175/2009JCLI2683.1.

——, T. J. Osborn, Y. Kushnir, I. R. Simpson, J. Nakamura, and H. Liu, 2019: Climate variability and change of Mediterranean-type climates. *J. Climate*, **32**, 2887–2915, https://doi.org/10.1175/JCLI-D-18-0472.1.

Seneviratne, S. I., 2012: Historical drought trends revisited. *Nature*, **491**, 338–339, https://doi.org/10.1038/491338a.

Sheffield, J., E. F. Wood, and M. L. Roderick, 2012: Little change in global drought over the past 60 years. *Nature*, **491**, 435–438, https://doi.org/10.1038/nature11575.

Slater, L. J., and Coauthors, 2021: Nonstationary weather and water extremes: A review of methods for their detection, attribution, and management. *Hydrol. Earth Syst. Sci.*, **25**, 3897–3935, https://doi.org/10.5194/hess-25-3897-2021.

Stagge, J. H., 2021: staggelab/spibayes: Pre-release version. Zenodo, https://doi.org/10.5281/zenodo.4927983.

——, and K. Sung, 2022: A Non-Stationary Standardized Precipitation Index (NSPI) using Bayesian splines. *J. Appl. Meteor. Climatol.*, **1**, https://doi.org/10.1175/JAMC-D-21-0244.1.

——, L. M. Tallaksen, C. Y. Xu, and H. A. J. van Lanen, 2014: Standardized Precipitation-Evapotranspiration Index (SPEI): Sensitivity to potential evapotranspiration model and parameters. *Hydrology in a Changing World: Environmental and Human Dimensions*, H. A. J. van Lanen and T. Daniell, Eds., International Association of Hydrological Sciences, 367–373, https://library.wur.nl/WebQuery/wurpubs/558281.

——, I. Kohn, L. M. Tallaksen, and K. Stahl, 2015a: Modeling drought impact occurrence based on meteorological drought indices in Europe. *J. Hydrol.*, **530**, 37–50, https://doi.org/10.1016/j.jhydrol.2015.09.039.

——, L. M. Tallaksen, L. Gudmundsson, A. F. Van Loon, and K. Stahl, 2015b: Candidate distributions for climatological drought indices (SPI and SPEI). *Int. J. Climatol.*, **35**, 4027–4040, https://doi.org/10.1002/joc.4267.

——, D. G. Kingston, L. M. Tallaksen, and D. M. Hannah, 2017: Observed drought indices show increasing divergence across Europe. *Sci. Rep.*, **7**, 14045, https://doi.org/10.1038/s41598-017-14283-2.

Stahle, D. W., 2020: Anthropogenic megadrought. *Science*, **368**, 238–239, https://doi.org/10.1126/science.abb6902.

Tallaksen, L., and H. A. J. van Lanen, 2004: *Hydrological Drought: Processes and Estimation Methods for Streamflow and Groundwater.* Elsevier, 579 pp.

Tibshirani, R., G. Walther, and T. Hastie, 2001: Estimating the number of clusters in a data set via the gap statistic. *J. Roy. Stat. Soc.*, **63**, 411–423, https://doi.org/10.1111/1467-9868.00293.

Trenberth, K. E., A. Dai, G. van der Schrier, P. D. Jones, J. Barichivich, K. R. Briffa, and J. Sheffield, 2014: Global warming and changes in drought. *Nat. Climate Change*, **4**, 17–22, https://doi.org/10.1038/nclimate2067.

Ukkola, A. M., M. G. D. Kauwe, M. L. Roderick, G. Abramowitz, and A. J. Pitman, 2020: Robust future changes in meteorological drought in CMIP6 projections despite uncertainty in precipitation. *Geophys. Res. Lett.*, **47**, e2020GL087820, https://doi.org/10.1029/2020GL087820..

Van Loon, A. F., S. W. Ploum, J. Parajka, A. K. Fleig, E. Garnier, G. Laaha, and H. J. Van Lanen, 2015: Hydrological drought types in cold climates: Quantitative analysis of causing factors and qualitative survey of impacts. *Hydrol. Earth Syst. Sci.*, **19**, 1993–2016, https://doi.org/10.5194/hess-19-1993-2015.

——, and Coauthors, 2016: Drought in a human-modified world: Reframing drought definitions, understanding, and analysis approaches. *Hydrol. Earth Syst. Sci.*, **20**, 3631–3650, https://doi.org/10.5194/hess-20-3631-2016.

Vicente-Serrano, S. M., S. Beguería, and J. I. López-Moreno, 2010: A multiscalar drought index sensitive to global warming: The Standardized Precipitation Evapotranspiration Index. *J. Climate*, **23**, 1696–1718, https://doi.org/10.1175/2009JCLI2909.1.

——, and Coauthors, 2021: Long-term variability and trends in meteorological droughts in western Europe (1851–2018). *Int. J. Climatol.*, **41**, E690–E717, https://doi.org/10.1002/joc.6719.

Wang, X., and Coauthors, 2013: A stepwise cluster analysis approach for downscaled climate projection—A Canadian case study. *Environ. Modell. Software*, **49**, 141–151, https://doi.org/10.1016/j.envsoft.2013.08.006.

Williams, A. P., and Coauthors, 2020: Large contribution from anthropogenic warming to an emerging North American megadrought. *Science*, **368**, 314–318, https://doi.org/10.1126/science.aaz9600.

Wood, S. N., 2004: Stable and efficient multiple smoothing parameter estimation for generalized additive models. *J. Amer. Stat. Assoc.*, **99**, 673–686, https://doi.org/10.1198/016214504000000980.

——, 2006: Low-rank scale-invariant tensor product smooths for generalized additive mixed models. *Biometrics*, **62**, 1025–1036, https://doi.org/10.1111/j.1541-0420.2006.00574.x.

——, 2011: Fast stable restricted maximum likelihood and marginal likelihood estimation of semiparametric generalized linear models. *J. Roy. Stat. Soc.*, **73B**, 3–36, https://doi.org/10.1111/j.1467-9868.2010.00749.x.

Wu, J., X. Chen, H. Yao, L. Gao, Y. Chen, and M. Liu, 2017: Non-linear relationship of hydrological drought responding to meteorological drought and impact of a large reservoir. *J. Hydrol.*, **551**, 495–507, https://doi.org/10.1016/j.jhydrol.2017.06.029.